Hindawi
Mathematical Problems in Engineering
Volume 2021, Article ID 8216439, 20 pages
https://doi.org/10.1155/2021/8216439

Research Article

Analysis of the Deep Sea Mining Pipe Transverse Vibration Characteristics Based on Finite Element Method

Linjing Xiao and Qiang Liu

College of Mechanical and Electronic Engineering, Shandong University of Science and Technology, Qingdao 266590, China

Correspondence should be addressed to Qiang Liu; qiangliu17@126.com

Received 5 August 2020; Revised 26 May 2021; Accepted 20 June 2021; Published 6 July 2021

Academic Editor: He Chen

This paper analyzes the transverse vibration laws of 5000 m ladder-shaped mining pipe under different towing velocities and accelerations in the ocean, thinking of the pipe as the beam model, discretized based on the FEM. The algorithm is used to solve the problem to obtain the transverse vibration law. The research shows that the mining pipe overall transverse vibration trend decreases first and then increases, the minimum vibration value occurs at 3000 m, and the maximum occurs at the top. Increasing the towing velocity, acceleration, and ore bin weight will increase the transverse vibration value. The vibration intensity produced by the same acceleration in the constant acceleration and deceleration stages is different, and the damping effect after adding the same damping is also different. In the range of 0.01 m/s^2–0.1 m/s^2, the vibration reduction effect after adding damping in the constant deceleration stage is more significant, and in the range of 0.1 m/s^2-0.2 m/s^2, the vibration reduction effect after adding damping in the constant acceleration stage is more significant. In the stage of the constant acceleration or deceleration, when adding the same damping, the vibration intensity generated by the large acceleration is still far greater than the vibration intensity generated by the small acceleration, so the mining ship should keep the small acceleration for towing motion.

1. Introduction

With the growth of the world population and the economy rapid development, the demand for metal mineral resources in various countries is increasing day by day [1]. Due to the increasing intensity of land resource development and the gradual decrease of rich ore deposits, the contradiction between the demand for mineral resources and the onshore reserves and the difficulty of exploitation is increasing [2]. The seabed contains rich mineral resources such as polymetallic nodules, sulfides, and polymetallic ooze. In addition, there are many strategic resources that have not been fully understood and utilized by humans [3]. If safe and efficient commercial mining can be realized and the impact on the marine ecological environment can be well controlled, the abundant marine minerals will become the alternative resources of onshore mineral resources and meet the economic development needs of human society in the future [4]. The deep sea mining system can collect polymetallic nodules on the sea floor and transport them back to the land by mining ships [5]. As the core component of the deep sea mining system, the mining pipe subsystem will undergo transverse vibration and deformation due to the combined action of waves and currents in the ocean [6]. In order to ensure the efficient operation of the mining system, it is necessary to minimize the impact of lateral vibration on the mining pipe system, so it is very meaningful to study the transverse vibration of the mining pipe.

American researcher Chung made an in-depth analysis of the spatial configuration, axial vibration, and transverse swing of the mining pipe under complex loads and studied the variation of the ocean current drag coefficient and Reynolds coefficient with the ocean depth [7]. Cheng studied the longitudinal vibration of the mining pipe. In order to reduce the longitudinal vibration, the pipe was optimized and the vibration damping device was added into the pipe. The research results showed that the dynamic response caused by external load excitation was weakened after the

addition of the vibration damping device [8]. Haluk used the separation variable method to study the longitudinal vibration of the ladder-shaped mining pipe with and without shock absorbers [9]. Based on the concentrated mass method and incremental iteration method, Sup Hong carried out the three-dimensional dynamic research on the mining pipe system of the deep sea mining and completed the axial forced vibration and three-dimensional nonlinear dynamic analysis of the mining pipe under the vertical state in the time domain [10]. Yoon Chi Ho used the finite element method to study the longitudinal vibration characteristics of the mining pipe and the interaction between the internal and external fluids and drew the conclusion that the longitudinal vibration of the mining pipe had negligible influence on the internal fluids [11]. Xu et al. established the double-Euler model to study the influence of transverse swing on the conveying characteristics of the mining pipe and concluded that the greater the transverse swing of the mining pipe, the more uneven the distribution of particles in the pipe and the more difficult to lift [12]. Li established the finite element analysis model for the 1000 m mining pipe and studied the influence of different working conditions and towing velocities on the transverse displacement of the mining pipe [13]. Liu et al. used the finite element method to study the transverse offset and deformation of the mining pipe in deep sea mining system, analyzed various factors affecting the transverse offset characteristics of the mining pipe, put forward the concept of "displacement lag period," and analyzed the relationship between the displacement lag period and towage acceleration [14]. Qiu applied Galerkin theory to analyze the longitudinal vibration of the mining pipe system and obtained the law of the longitudinal vibration amplitude changing with the wave frequency under different wave cycles [15].

In summary, there are many researches on the longitudinal vibration and transverse offset of the mining pipe, but few researches on the transverse vibration of the 5000 m mining pipe. The deep sea mining pipe is the problem of large displacement and small strain, while the deformation of the element and the angle between adjacent elements are changed to a small amount; the stress-strain relationship is still linear. In this paper, the 5000 m mining pipe is simplified into the nonlinear beam element; the total Lagrangian approach and the principle of virtual displacement are used for linear processing. And the finite element method is used for dynamic theoretical analysis, using Wilson-θ algorithm for numerical calculation. The transverse vibration characteristics of the mining pipe under different towing velocities and accelerations of the mining ship are studied. The main content of the research can provide useful reference for the choice of mining ship towing velocity and the design of the overall mining system.

2. Physical Modeling

The structural diagram of the deep sea mining system is shown in Figure 1. It is mainly composed of mining pipe subsystem, mineral collection subsystem, and mining ship [16]. The mining pipe subsystem mainly includes the mining pipe, lifting pump group, middle ore bin, and shock absorber

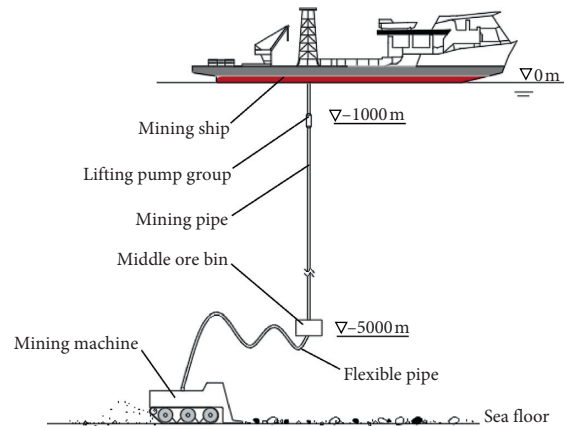

Figure 1: Structure diagram of the deep sea mining system.

[17]. The mineral collection subsystem includes the mining machine and the flexible pipe. The flexible pipe can play the buffering role [18]. The mining machine is used to collect nodules resources from the seabed and transport them to the middle ore bin through the flexible pipe. Under the action of the lifting pump group, nodules in the ore bin are transported to the mining ship through the mining pipe, and then the nodules resources are transported back to the land by the mineral transfer ship.

As shown in Figure 2, the mining pipe subsystem is an important part of the deep sea mining system, which undertakes the task of transporting the nodules collected by the seabed mining machine to the surface mining ship, and is also the installation carrier of cables and power components [19]. The length of the mining pipe is thousands of meters. Under the action of the mining ship's towing velocity, the external sea currents, waves, and other complex loads, it is easy to produce large transverse vibration and deformation, resulting in pipeline failure, affecting the mining efficiency of the whole deep sea mining system, and even causing major safety accidents [20]. Therefore, it is necessary to research the transverse vibration characteristics of the mining pipe. In order to reduce the load borne by the mining pipe, the ladder-shaped mining pipe is adopted, which is divided into four steps. The diameter of the pipe decreases from top to bottom. The top of the mining pipe is connected with the mining ship and performs heave motion ($u(t)$) together [21].

3. Theoretical Analysis

The basic idea of the finite element method is to discretize the continuous solution area into a group of finite elements connected together in a certain way [22]. Because the elements can be combined according to different connection modes and the elements themselves can have different shapes, so it is possible to model the solution domain with complex geometric shapes [23]. Another important feature of the finite element method as a numerical analysis method is to use the approximate function in each element to represent the unknown field function to be solved in the full-solution domain [24]. The approximate function in the element is usually expressed by the value of its derivative and

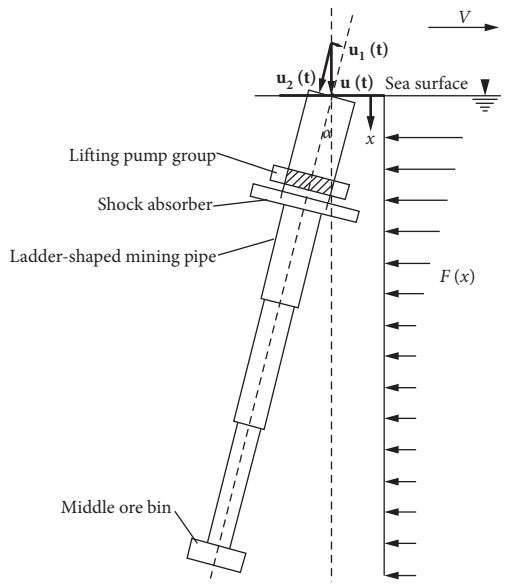

Figure 2: Schematic diagram of the mining pipe subsystem.

the interpolation function; in this way, a continuous infinite degree of freedom problem becomes a discrete finite degree of freedom problem [25]. The biggest advantage of the discontinuous FEM is that it has low requirements on the smoothness of the solution and the best convergence, and it can also make high-precision simulations of some discontinuous physical phenomena [26]. The discontinuous FEM is widely used in fluid dynamics and solid mechanics. For example, the propagation of heat conduction in the medium will produce parabolic problems with discontinuous coefficients; their solutions and energy flow meet the continuity at the interface, so the discontinuous FEM can effectively solve the problem [27].

3.1. Mining Ship Movement. The heave motion of the mining ship can be approximated to simple harmonic motion, and the motion period is equal to the wave period; then, the heave motion equation is expressed as follows [28]:

$$u(t) = z_{sa} \sin(\omega t), \tag{1}$$

where z_{sa} is the heave amplitude of the mining ship.

Moore's empirical formula is used to calculate the heave amplitude of the mining ship, and the calculation formula is as follows [29]:

$$z_{sa} = A_0 + A_1 C_w + A_2 C_B + A_3 \frac{L_{OA}}{B} + A_4 \frac{h}{L_{OA}} + A_5 L_{CB} + A_6 \frac{K_{YY}}{L_{OA}} + A_7 \frac{V}{\sqrt{L_{OA}}}, \tag{2}$$

where $A_0 - A_7$ is the coefficient that varies with classification and ship length; C_w is the waterplane coefficient; C_B is the square coefficient; L_{OA} is the length of the mining ship; B is the width of the ship; h is the depth of draft; L_{CB} is the longitudinal position of the ship buoyancy center; K_{YY} is the ship's longitudinal mass inertia radius; V is the towing velocity of the mining ship; and M_a is the displacement of the mining ship.

3.2. Beam Element Analysis. The mining pipe is simplified as the beam unit [30], taking any small beam element in the three-dimensional space, as shown in Figure 3. Setting the nodes at both ends as i and j, u, v, and w represent the linear displacement component in three directions, respectively. θ is the angular component; then, the element node displacement vector is $[\xi] = \left[u_i \;\; v_i \;\; w_i \;\; \theta_{ix} \;\; \theta_{iy} \;\; \theta_{iz} \;\; u_j \;\; v_j \;\; w_j \;\; \theta_{jx} \;\; \theta_{jy} \;\; \theta_{jz} \right]^T$.

Hermite interpolation function is as follows [31]:

$$N_1 = 1 - \frac{x}{l}, \tag{3}$$

$$N_2 = \frac{x}{l}, \tag{4}$$

$$N_3 = 1 - \frac{3x^2}{l^2} + \frac{2x^3}{l^3}, \tag{5}$$

$$N_4 = x - \frac{2x^2}{l} + \frac{x^3}{l^2}, \tag{6}$$

$$N_5 = \frac{3x^2}{l^2} - \frac{2x^3}{l^3}, \tag{7}$$

$$N_6 = -\frac{x^2}{l^2} + \frac{x^3}{l^3}. \tag{8}$$

In equations (3)–(8), l is the beam element length.

The element node displacement function is as follows:

$$u = N_1 u_i + N_2 u_j, \tag{9}$$

$$v = N_3 v_i + N_4 \theta_{iz} + N_5 v_j + N_6 \theta_{jz}, \tag{10}$$

$$w = N_3 w_i - N_4 \theta_{iy} + N_5 w_j - N_6 \theta_{jy}, \tag{11}$$

$$\theta = N_1 \theta_{ix} + N_2 \theta_{jx}. \tag{12}$$

The geometric equation corresponding to the beam element is as follows:

$$\{\gamma\} = \left\{ \varepsilon_x \;\; \gamma_z \;\; \gamma_y \;\; \gamma_x \right\}^T = \begin{Bmatrix} \dfrac{\mathrm{d}u}{\mathrm{d}x} \\ -\dfrac{\mathrm{d}^2 v}{\mathrm{d}x^2} \\ -\dfrac{\mathrm{d}^2 w}{\mathrm{d}x^2} \\ \dfrac{\mathrm{d}\theta}{\mathrm{d}x} \end{Bmatrix}, \tag{13}$$

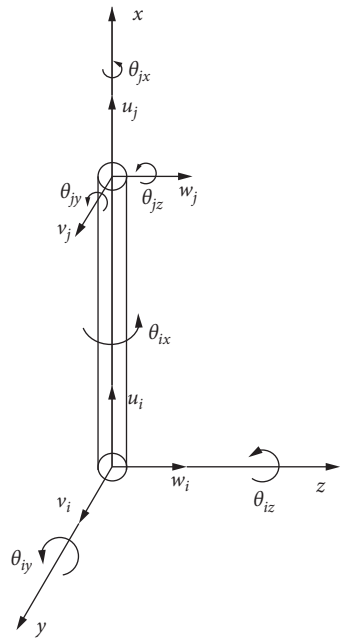

Figure 3: The beam element node displacement.

where ε_x is the axial strain of beam element, γ_z is the curvature of the beam element deflection curve in the coordinate plane oxy, γ_y is the curvature of the beam element deflection curve in the coordinate plane oxz, and γ_x is the torsion rate.

Substituting equations (9)–(12) into equation (13), the geometric matrix can be obtained, which is expressed as follows:

$$[B] = \begin{bmatrix} N_1' & 0 & 0 & 0 & 0 & 0 & N_2' & 0 & 0 & 0 & 0 & 0 \\ 0 & -N_3'' & 0 & 0 & 0 & -N_4'' & 0 & -N_5'' & 0 & 0 & 0 & -N_6'' \\ 0 & 0 & -N_3'' & 0 & N_4'' & 0 & 0 & 0 & -N_5'' & 0 & N_6'' & 0 \\ 0 & 0 & 0 & N_1' & 0 & 0 & 0 & 0 & 0 & N_2' & 0 & 0 \end{bmatrix}. \tag{14}$$

The element stress is expressed as follows:

$$\sigma = [H]\gamma,$$
$$[H] = \begin{bmatrix} EA & 0 & 0 & 0 \\ 0 & EI_z & 0 & 0 \\ 0 & 0 & EI_y & 0 \\ 0 & 0 & 0 & GJ \end{bmatrix}, \tag{15}$$

where E is the elastic modulus; A is the cross sectional area; I_z is the inertia moment of the cross section towards the neutral axis oz; I_y is the inertia moment of the cross section towards the neutral axis oy; G is the shear modulus; and J is the polar inertia moment of the cross section towards the ox axis.

The virtual work equation of the beam element, that is, the virtual work of the element node force is equal to its internal force virtual work:

$$[\xi]^{*T} F = \int [\gamma]^{*T} \sigma \mathrm{d}x, \tag{16}$$

where $*$ is the virtual displacement.

That is,

$$[\xi]^{*T} F = \int [\xi]^{*T} \cdot [B]^T [H][B][\xi]\mathrm{d}x,$$
$$F = [K^e][\xi]. \tag{17}$$

So, the calculation formula of element stiffness matrix is as follows:

$$[K^e] = \int [B]^T [H][B]\mathrm{d}v. \tag{18}$$

Similarly, the expression formula of element mass matrix is as follows:

$$[M^e] = \int m_h [N]^T [N]\mathrm{d}x, \tag{19}$$

$$[N] = \begin{bmatrix} N_1 & 0 & 0 & 0 & 0 & 0 & N_2 & 0 & 0 & 0 & 0 & 0 \\ 0 & N_3 & 0 & 0 & 0 & N_4 & 0 & N_5 & 0 & 0 & 0 & N_6 \\ 0 & 0 & N_3 & 0 & -N_4 & 0 & 0 & 0 & N_5 & 0 & -N_6 & 0 \\ 0 & 0 & 0 & N_1 & 0 & 0 & 0 & 0 & 0 & N_2 & 0 & 0 \end{bmatrix}. \tag{20}$$

In equation (19), m_h is the weight of the mining pipe per unit length. The element stiffness matrix and mass matrix can be calculated by equations (19) and (20) as follows:

$$K^e = \frac{1}{l^3}\begin{bmatrix}
EAl^2 & 0 & 0 & 0 & 0 & 0 & -EAl^2 & 0 & 0 & 0 & 0 & 0 \\
0 & 12EI_z & 0 & 0 & 0 & 6EI_z l & 0 & -12EI_z & 0 & 0 & 0 & 6EI_z l \\
0 & 0 & 12EI_y & 0 & -6EI_y l & 0 & 0 & 0 & -12EI_y & 0 & -6EI_y l & 0 \\
0 & 0 & 0 & GJl^2 & 0 & 0 & 0 & 0 & 0 & -GJl^2 & 0 & 0 \\
0 & 0 & -6EI_y l & 0 & 4EI_y l^2 & 0 & 0 & 0 & 6EI_y l & 0 & 2EI_y l^2 & 0 \\
0 & 6EI_z l & 0 & 0 & 0 & 4EI_z l^2 & 0 & -6EI_z l & 0 & 0 & 0 & 2EI_z l^2 \\
-EAl^2 & 0 & 0 & 0 & 0 & 0 & EAl^2 & 0 & 0 & 0 & 0 & 0 \\
0 & -12EI_z & 0 & 0 & 0 & -6EI_z l & 0 & 12EI_z & 0 & 0 & 0 & -6EI_z l \\
0 & 0 & -12EI_y & 0 & 6EI_y l & 0 & 0 & 0 & 12EI_y & 0 & 6EI_y l & 0 \\
0 & 0 & 0 & -GJl^2 & 0 & 0 & 0 & 0 & 0 & GJl^2 & 0 & 0 \\
0 & 0 & -6EI_y l & 0 & 2EI_y l^2 & 0 & 0 & 0 & 6EI_y l & 0 & 4EI_y l^2 & 0 \\
0 & 6EI_z l & 0 & 0 & 0 & 2EI_z l^2 & 0 & -6EI_z l & 0 & 0 & 0 & 4EI_z l^2
\end{bmatrix},$$

$$M^e = \frac{\rho Al}{420}\begin{bmatrix}
140 & 0 & 0 & 0 & 0 & 0 & 70 & 0 & 0 & 0 & 0 & 0 \\
0 & 156 & 0 & 0 & 0 & 22l & 0 & 54 & 0 & 0 & 0 & -13l \\
0 & 0 & 156 & 0 & -22l & 0 & 0 & 0 & 54 & 0 & 13l & 0 \\
0 & 0 & 0 & \frac{140J}{A} & 0 & 0 & 0 & 0 & 0 & \frac{70J}{A} & 0 & 0 \\
0 & 0 & -22l & 0 & 4l^2 & 0 & 0 & 0 & -13l & 0 & -3l^2 & 0 \\
0 & 22l & 0 & 0 & 0 & 4l^2 & 0 & 13l & 0 & 0 & 0 & -3l^2 \\
70 & 0 & 0 & 0 & 0 & 0 & 140 & 0 & 0 & 0 & 0 & 0 \\
0 & 54 & 0 & 0 & 0 & 13l & 0 & 156 & 0 & 0 & 0 & -22l \\
0 & 0 & 54 & 0 & -13l & 0 & 0 & 0 & 156 & 0 & 22l & 0 \\
0 & 0 & 0 & \frac{70J}{A} & 0 & 0 & 0 & 0 & 0 & \frac{140J}{A} & 0 & 0 \\
0 & 0 & 13l & 0 & -3l^2 & 0 & 0 & 0 & 22l & 0 & 4l^2 & 0 \\
0 & -13l & 0 & 0 & 0 & -3l^2 & 0 & -22l & 0 & 0 & 0 & 4l^2
\end{bmatrix}. \tag{21}$$

For the mining pipe subsystem, there is the mixture of mineral fluid inside the pipe and additional weight outside the pipe during operation, so the unit mass matrix should be modified, matrix element $M^e(1,1)$, $M^e(1,7)$, $M^e(7,1)$, $M^e(7,7)$, $M^e(4,4)$, $M^e(10,10)$, $M^e(4,10)$, $M^e(10,4)$ are multiplied by factor λ, and the final unit mass matrix is expressed as follows [32]:

$$M^e = \frac{\rho A l}{420}\begin{bmatrix} 140\lambda & 0 & 0 & 0 & 0 & 0 & 70\lambda & 0 & 0 & 0 & 0 & 0 \\ 0 & 156 & 0 & 0 & 0 & 22l & 0 & 54 & 0 & 0 & 0 & -13l \\ 0 & 0 & 156 & 0 & -22l & 0 & 0 & 0 & 54 & 0 & 13l & 0 \\ 0 & 0 & 0 & \frac{140J\lambda}{A} & 0 & 0 & 0 & 0 & 0 & \frac{70J\lambda}{A} & 0 & 0 \\ 0 & 0 & -22l & 0 & 4l^2 & 0 & 0 & 0 & -13l & 0 & -3l^2 & 0 \\ 0 & 22l & 0 & 0 & 0 & 4l^2 & 0 & 13l & 0 & 0 & 0 & -3l^2 \\ 70\lambda & 0 & 0 & 0 & 0 & 0 & 140\lambda & 0 & 0 & 0 & 0 & 0 \\ 0 & 54 & 0 & 0 & 0 & 13l & 0 & 156 & 0 & 0 & 0 & -22l \\ 0 & 0 & 54 & 0 & -13l & 0 & 0 & 0 & 156 & 0 & 22l & 0 \\ 0 & 0 & 0 & \frac{70J\lambda}{A_t} & 0 & 0 & 0 & 0 & 0 & \frac{140J\lambda}{A} & 0 & 0 \\ 0 & 0 & 13l & 0 & -3l^2 & 0 & 0 & 0 & 22l & 0 & 4l^2 & 0 \\ 0 & -13l & 0 & 0 & 0 & -3l^2 & 0 & -22l & 0 & 0 & 0 & 4l^2 \end{bmatrix}, \tag{22}$$

$$\lambda = \frac{M_{\text{in}} + M_h + m_h}{M_{\text{in}} + M_h + M_{\text{add}} + m_h},$$

where M_{in} is the fluid mass in the pipeline of unit length, M_h is the additional hardware weight per unit length of pipe, and M_{add} is the additional weight of seawater.

3.3. Overall Matrix Analysis. In order to reduce the load borne by the mining pipe, the ladder-shaped mining pipe is adopted and divided into four steps according to its diameter. The total length is 5000 m and is divided into 200 units, each unit is 25 m long, and there are the total of 201 nodes, as shown in Figure 4. Each node contains 6 degrees of freedom, so there are 1206 degrees of freedom in total. The total stiffness matrix K is 1206×1206.

The nth element stiffness matrix is $K^{e(n)}$, and n is the unit number 1, 2,. . ., 200. The submatrix can be expressed as $k_{rs}^{(n)}$, and r and s range from 1 to 12. The element k_{77}^n in the stiffness matrix of the nth element is added to the element $k_{11}^{(n+1)}$ in the stiffness matrix of the $(n+1)$th element, taking this as the registration point, and the corresponding items are added after overlapping. The overall stiffness matrix is as follows:

$$K = \begin{bmatrix} k_{11} & k_{12} & \cdots & k_{1,1205} & k_{1,1206} \\ \vdots & & & & \vdots \\ \vdots & & k_{pq} & & \vdots \\ k_{1206,1} & k_{1206,2} & \cdots & k_{1206,1205} & k_{1206,1206} \end{bmatrix}. \tag{23}$$

In the same way, the element m_{77}^n in the nth element mass matrix and the element $m_{11}^{(n+1)}$ in the $(n+1)$th element mass matrix are added, taking this as the registration point, and the corresponding items are added after overlapping. The overall mass matrix is as follows:

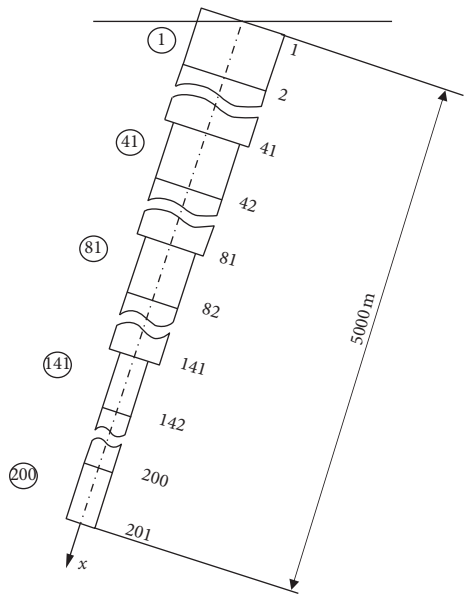

Figure 4: Finite element discrete schematic diagram of the mining pipe.

$$M = \begin{bmatrix} m_{11} & m_{12} & \cdots & m_{1,1205} & m_{1,1206} \\ \vdots & & & & \vdots \\ \vdots & & m_{pq} & & \vdots \\ m_{1206,1} & m_{1206,2} & \cdots & m_{1206,1205} & m_{1206,1206} \end{bmatrix}. \quad (24)$$

3.4. Load Analysis. In the marine environment, the wave and ocean current exist together, and the ocean current can cause the pipe deviation, and the wave can cause the pipe transverse vibration. According to the Morison equation, the ocean hydrodynamic force under the combined action of wave and current is composed of velocity force and inertial force [33].

$$F = F_D + F_M, \quad (25)$$

where F_D is the velocity force vector and F_M is the inertial force vector.

$$F_D = F_n + F_t, \quad (26)$$

where F_n is the normal velocity force and F_t is the tangential velocity force. The calculation formula is as follows:

$$\begin{aligned} F_n &= \frac{1}{2} C_D D \rho_w v_{sv}^2 \cos^2 \alpha, \\ F_t &= \frac{\pi}{2} C_t D \rho_w v_{sv}^2 \sin^2 \alpha. \end{aligned} \quad (27)$$

The inertial force calculation formula is as follows:

$$\begin{aligned} F_M &= \frac{\pi}{4} C_M D^2 \rho_w v_{sv}' \cos \alpha, \\ v_{sv} &= v_{wv} + v_c + v_p, \\ v_c &= 0.15 + 1.6 \times \left(\frac{5000 + x}{5000} \right)^{12}, \\ v_{wv} &= \frac{H_w}{2} \omega e^{k_w x} \sin(k_w z - \omega t), \\ k_w &= \frac{2\pi}{\lambda_w}, \\ \lambda_w &= \frac{T^2 g}{2\pi}, \\ \omega &= \frac{2\pi}{T}, \end{aligned} \quad (28)$$

where C_D is the normal resistance coefficient, and the value is 1.2 [34]; C_t is the tangential resistance coefficient, which is generally 30 to 120 times smaller than the normal resistance coefficient [35]; C_M is the coefficient of inertial resistance, and the value is 2.0 [36];D is the external diameter of the pipeline; ρ_w is the density of seawater; v_{sv} is the relative velocity vector between seawater and pipeline; v_{wv} is the fluid velocity vector under wave action; v_c is the fluid velocity vector under the action of ocean current; v_p is the velocity vector of pipe movement; x is the water depth, the ocean surface is 0, and the downward value is negative; H_w is the height of the wave; k_w is the wave number; λ_w is the wavelength; ω is the wave motion frequency; and T is the period of wave motion.

Taking the moment from the top of the mining pipe, the calculation formula for the angle of the mining pipe is as follows [37]:

$$\int_0^L Fx\mathrm{d}x - \int_0^L m_h g x \sin \alpha \mathrm{d}x - mgL \sin \alpha = 0, \quad (29)$$

where m is the weight of the middle ore bin and L is the length of the mining pipe.

Then the external force matrix is as follows:

$$F(t) = \left[F(t_1) \;\; 0 \;\; 0 \;\; \cdots \;\; \cdots \;\; 0 \;\; 0 \;\; 0 \right]^T. \quad (30)$$

The node load force is as follows:

$$\begin{aligned} F(t_1) &= F_D \sin \alpha \sin \omega t, \\ F_D &= M \omega^2 z_{sa}. \end{aligned} \quad (31)$$

3.5. Equation Solving. The dynamic equation of the system is as follows [38]:

$$M\zeta'' + C\zeta' + K\zeta = F(t), \quad (32)$$

where C is the damping matrix. The damping of the structure is generally difficult to accurately determine, in practice, the approximate value of the damping often given by the measured data. Therefore, the overall damping matrix of the structure can be directly given, here setting as the form of the viscous damping coefficient c and the matrix product [39].

The initial state is as follows:

$$\begin{aligned} \zeta(x,0) &= u_1, \\ \zeta'(x,0) &= u_1'. \end{aligned} \tag{33}$$

The Wilson-θ direct integration method is used to obtain the recursive formula of node displacement and velocity; the calculation formula is as follows [40]:

$$\zeta(t+\Delta t) = \zeta_t + \zeta_t' \Delta t + \frac{\Delta t^2}{6}\left(\zeta_{t+\Delta t}'' + 2\zeta_t''\right), \tag{34}$$

$$\zeta'(t+\Delta t) = \zeta_t' + \frac{\Delta t}{2}\left(\zeta_{t+\Delta t}'' + \zeta_t''\right), \tag{35}$$

$$\zeta''(t+\Delta t) = \zeta_t'' + \frac{1}{\theta}\left(\zeta_{t+\theta\Delta t}'' - \zeta_t''\right). \tag{36}$$

Iterative solution is required from time t to Δt. The new state quantity is iterated according to (34)–(36), and the displacement, velocity, and acceleration at the next moment can be obtained, until the displacement and velocity of the whole time are obtained and the iterative operation is completed.

4. Results and Discussion

When the deep sea mining system is working, the mining ship will adjust towing velocity as needed. At the beginning, the velocity of the mining ship is 0 m/s; then, it accelerates to the set constant towing velocity, and, at the end, the towing velocity gradually slows down to 0 m/s. In this process, the transverse vibration response of the mining pipe is directly related to the towing process of the mining ship, and the whole towing process is shown in Figure 5. w is the variation law of towing velocity with time, $0 - t_1$ is the constant acceleration stage, $t_1 - t_2$ is the constant towing stage, $t_2 - t_3$ is the constant deceleration stage, and V is the constant towing velocity.

The 5000 m mining pipe is divided into four steps with lengths of 1000 m, 1000 m, 1500 m, and 1500 m, respectively. The specific parameters are shown in Tables 1 and 2. The transverse vibration characteristics of mining pipe under different velocities and acceleration are analyzed and the corresponding results are obtained.

4.1. Natural Frequency Calculation. The upper end of the mining pipe is connected with the mining ship and moves with the ship. The tail end is connected with the middle ore bin. The shock absorber is installed at 1000 m underwater to provide controllable damping c. Because the length of the mining pipe is much greater than the thickness of the pipe joint, only the weight of the mining pipe is considered here [41]. The mining machine is connected with the middle ore bin through the mining flexible pipe, and the flexible pipe has less rigidity and is supported by buoyant materials, so the force on the mining pipe can be ignored [42]. Regarding the lower end of the mining pipe as the free end, the natural frequency calculation formula is as follows [43]:

$$\det\left(K - f^2 M\right) = 0. \tag{37}$$

After calculation, the first 20 order natural frequency values of the mining pipe are shown in Table 3.

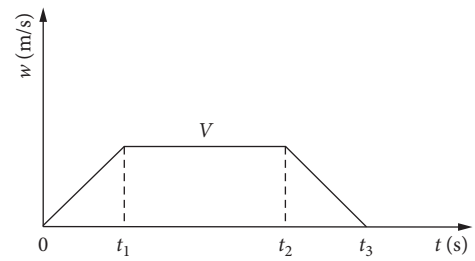

Figure 5: The mining ship towing process diagram.

Table 1: Related parameters of the mining pipe subsystem.

Ladder section	1	2	3	4
L/(m)	1 000	1 000	1 500	1 500
D_2/(m)	0.28	0.26	0.24	0.22
D_1/(m)	0.20	0.20	0.20	0.20
m_h/(kg/m)	236.63	170.08	108.46	51.76
A_h/(m^2)	0.0302	0.0217	0.0139	0.0066
I_z/(m^4)	2.230×10^{-4}	1.457×10^{-4}	8.430×10^{-5}	3.643×10^{-5}
J/(m^4)	4.460×10^{-4}	2.914×10^{-4}	1.686×10^{-4}	7.286×10^{-5}
E/(GPa)	210	210	210	210
G/(GPa)	84	84	84	84

Table 2: Table of wave characteristics.

Working wind condition	H_w/(m)	T (s)
Level 4	3.5	8.8
Level 6	6.0	5.8

4.2. Towing Velocity 0 and Transverse Vibration Analysis of the Mining Pipe

(i) Under the working wind condition of level 6, when the towing velocity of the mining ship is 0, the weight of the middle ore bin is 30 t, and the damping is 200 N · s/m. The transverse vibration law of the mining pipe is shown in Figure 6.

It can be seen from Figures 6(a)–6(d) that the transverse vibration of the mining pipe is irregular, and the maximum amplitude of vibration in each period is different, presenting an oscillation phenomenon. The maximum vibration amplitude of the mining pipe at 1000 m–5000 m first decreases and then increases, and the minimum vibration

Table 3: The first 20 order natural frequencies.

Order number	Natural frequency (Hz)	Order number	Natural frequency (Hz)
1	0.02817	11	0.03945
2	0.02886	12	0.0399
3	0.02959	13	0.04006
4	0.03047	14	0.04184
5	0.03144	15	0.04258
6	0.03319	16	0.04357
7	0.03417	17	0.04453
8	0.03698	18	0.04579
9	0.03866	19	0.04694
10	0.03881	20	0.0484

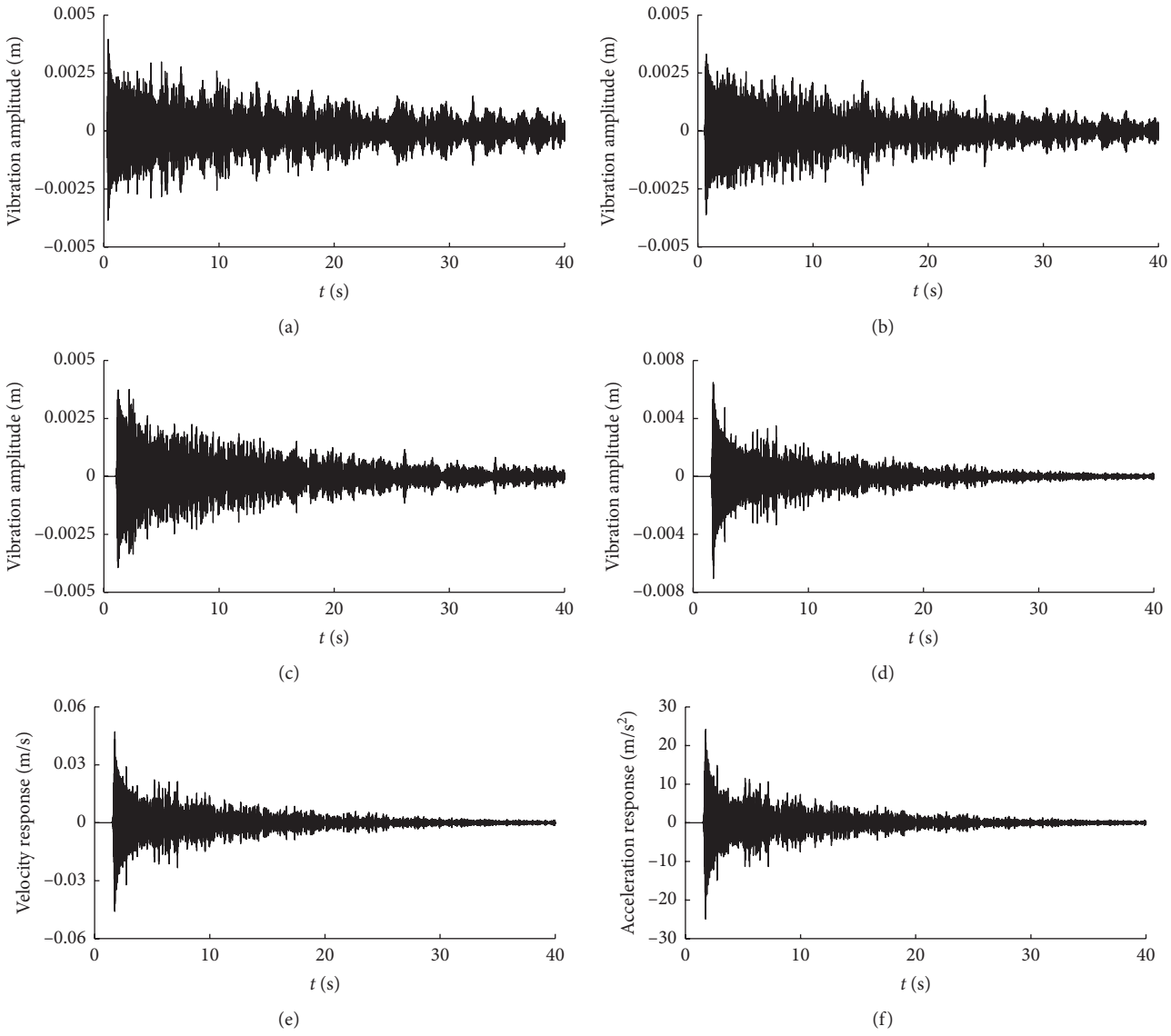

Figure 6: Transverse vibration response diagram of the mining pipe. (a) Displacement vibration response of the mining pipe at 1000 m. (b) Displacement vibration response of the mining pipe at 2000 m. (c) Displacement vibration response of the mining pipe at 3500 m. (d) Displacement vibration response of the mining pipe at 5000 m. (e) Velocity response of the mining pipe at 5000 m. (f) Acceleration response of the mining pipe at 5000 m.

amplitude appears in the third step; that is, the minimum vibration amplitude appears at a place between 2000 m and 3500 m of the mining pipe, and the vibration amplitude at the tail end of the mine pipe is smaller than the vibration amplitude at the top end. It can be seen from Figures 6(e) and 6(f) that the transverse vibration velocity and acceleration of the mining pipe are both of irregular motion and hysteresis response will occur. With the increase of pipeline depth, the hysteresis time of the mining pipe vibration displacement, velocity, and acceleration are increased.

(ii) Under the working wind condition of level 6, when the weight of the ore bin is 0 t, 30 t, 50 t, and 80 t, respectively, the towing velocity of the mining ship is 0 m/s and the damping is 200 N · s/m. The maximum vibration amplitude, maximum velocity amplitude, and maximum acceleration amplitude at the pipe different positions are shown in Figures 7–9.

It can be seen from Figure 7 that the overall maximum transverse vibration amplitude of the mining pipe decreases first and then increases from top to bottom; the maximum vibration amplitude appears at the top, the minimum vibration amplitude appears at 3000 m of the mining pipe, and the maximum vibration amplitude gradually decreases at 0–3000 m of the mining pipe. This is because the diameter of the mining pipe at 0–3000 m is large, the contact area between each node is large, the acting force is strong, the inertial force is weak, and the energy consumed is large, so the vibration amplitude gradually decreases. The maximum vibration amplitude of the mining pipe at 3000 m–5000 m increases gradually, because the diameter of the pipe becomes smaller, the contact area between each node decreases, the acting force weakens, the energy consumed decreases, and the inertial force increases, so the vibration amplitude tends to increase. Increasing the ore bin weight will increase the total weight of the mining ship, and the incentive on the upper end of the mining pipe will increase. Secondly, the structure of the mining pipe itself has not changed, the energy consumed by the interaction between nodes has not increased, and the inertia effect is enhanced; therefore, increasing the ore bin weight will increase the pipe overall transverse vibration amplitude, while the situation is the opposite when decreasing the ore bin weight. As shown in Figures 8 and 9, the amplitude of transverse maximum vibration velocity and acceleration of the mining pipe also decreases first and then increases. The maximum response appears at the top and the minimum response appears at 3000 m of the mining pipe, indicating that the vibration amplitude of the mining pipe changes slowly at 3000 m.

4.3. Transverse Vibration Analysis of the Mining Pipe under Different Constant Towing Velocities. Under the working wind condition of level 6, when the towing velocity of the mining ship is 0 m/s, 0.2 m/s, 0.5 m/s, 1.0 m/s, and 1.5 m/s, the weight of the ore bin is 30 t and the damping is 200 N · s/m. The maximum vibration amplitude at different positions of the mining pipe is shown in Figure 10.

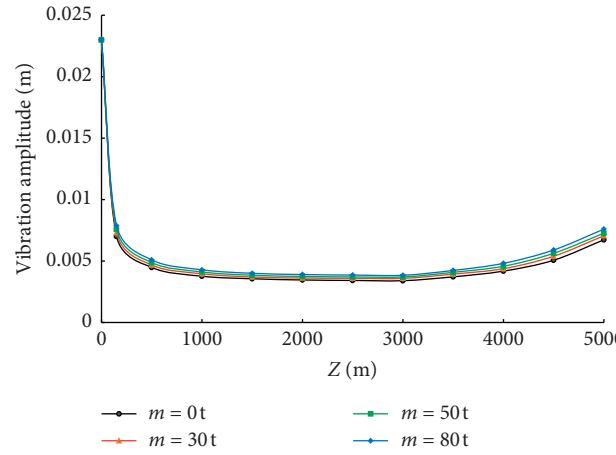

Figure 7: The variation law of the maximum transverse vibration amplitude.

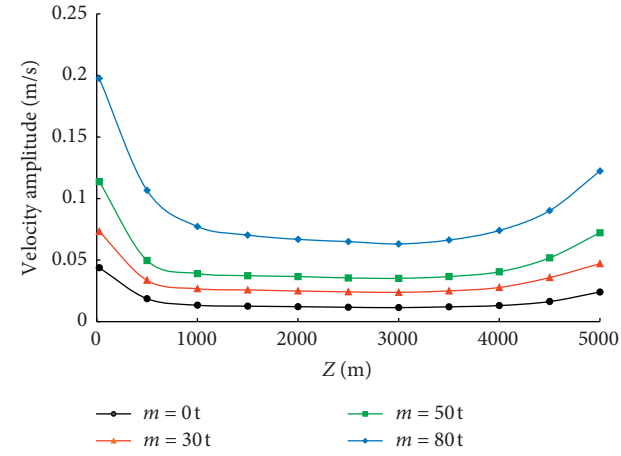

Figure 8: The variation law of the maximum velocity response amplitude.

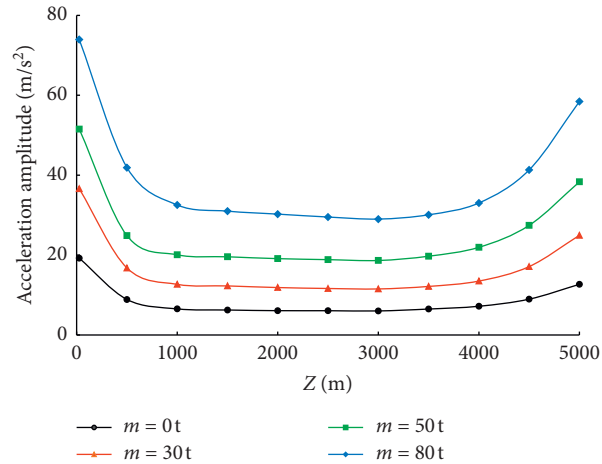

Figure 9: The variation law of the maximum acceleration response amplitude.

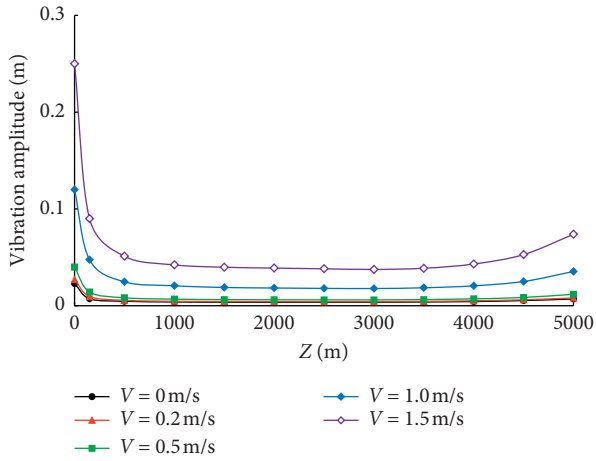

Figure 10: Variation law of the maximum vibration amplitude of mining pipe with different towing velocities.

As shown in Figure 10, the change of the towing velocities cannot change the transverse vibration law of the mining pipe that decreases first and then increases, and the minimum vibration amplitude still appears at 3000 m. When the towing velocity increases, the overall transverse vibration amplitude of the mining pipe will increase, and the greater the towing velocity is, the more obvious the increase of the overall vibration amplitude is. This is because when the mining ship towing velocity increases, the relative velocity between the mining pipe and the sea water will increase, causing the increase of the transverse offset angle. The component force applied to the top of the mining pipe in the normal direction increases, and the axial force decreases; however, the energy consumed by the interaction between nodes has not changed, and the transverse excitation load is increased. Therefore, increasing the towing velocity will increase the pipe overall transverse amplitude. And the larger the towing velocity is, the greater the amplitude of transverse vibration is, while the situation is the opposite when decreasing the ship towing velocity.

4.4. Transverse Vibration Analysis of the Mining Pipe under Different Towing Accelerations. Under the working wind condition of level 6, when the towing acceleration of the mining ship is 0 m/s^2, 0.01 m/s^2, 0.05 m/s^2, 0.1 m/s^2, 0.2 m/s^2, the weight of the ore bin is 30 t and the damping is 200 N · s/m. The maximum vibration amplitude at different positions of the mining pipe is shown in Figure 11.

Figure 11(a) shows the variation law of the mining pipe maximum transverse vibration amplitude under different accelerations during the towing acceleration stage of the mining ship, and Figure 11(b) shows the variation law of the mining pipe maximum transverse vibration amplitude under different accelerations during the towing deceleration stage of the mining ship. As shown in Figures 11(a) and 11(b), the change of acceleration cannot change the transverse vibration law of the mining pipe that first decreases and then increases. The maximum vibration amplitude appears at the top of the mining pipe, and the minimum vibration amplitude appears at 3000 m, but the increase of acceleration can increase the overall transverse vibration amplitude of the mining pipe. This is because when the towing acceleration increases, the relative acceleration between the mining pipe and the seawater will increase, and the external inertial force will strengthen, which will intensify the transverse oscillation of the mining pipe and increase the vibration amplitude. Therefore, the mining ship should try to keep a small acceleration to speed up or speed down.

4.5. Transverse Vibration Frequency Analysis

(i) Under the working wind condition of level 6, when the weight of the ore bin is 30 t, the towing velocity is 0 m/s, 0.2 m/s, 0.5 m/s, and 1.0 m/s respectively, and the damping is 200 N · s/m. The transverse vibration frequency of the mining pipe is shown in Figure 12.

As shown in Figure 12, the transverse vibration intensity of the mining pipe increases with the increase of towing velocity, but the change of towing velocity cannot change the transverse vibration frequency of the mining pipe. The vibration intensity corresponding to the first five order vibration frequencies of the mining pipe is relatively large, and the maximum vibration intensity appears at the second order vibration frequency (0.0315 Hz). When the towing velocity is 0 m/s, 0.2 m/s, 0.5 m/s, and 1.0 m/s, the corresponding maximum vibration intensity is 0.2716 dB, 0.3145 dB, 0.4659 dB, and 1.3978 dB, respectively.

(ii) Under the working wind condition of level 6, when the weight of the ore bin is 30 t, the towing acceleration is 0 m/s^2, 0.01 m/s^2, 0.05 m/s^2, 0.1 m/s^2, and 0.2 m/s^2, and the damping is 200 N · s/m. The transverse vibration frequency of the mining pipe is shown in Figure 13.

As shown in Figure 13, with the towing acceleration increase, the vibration intensity of the mining pipe is enhanced. Similarly, towing acceleration cannot change the frequency of transverse vibration, and the maximum vibration intensity appears at the second order vibration frequency. When the towing acceleration is 0 m/s^2, 0.01 m/s^2, 0.05 m/s^2, 0.1 m/s^2, and 0.2 m/s^2, the corresponding maximum vibration intensity at the acceleration stage is 0.2715 dB, 0.3145 dB, 0.4543 dB, 0.6406 dB, and 1.0251 dB, respectively. The corresponding maximum vibration intensity at the deceleration stage is 0.4659 dB, 0.5125 dB, 0.5591 dB, 0.6174 dB, and 0.7804 dB, respectively.

(iii) The first three order vibration frequencies are selected as the research object, and the corresponding frequencies are 0.0297 Hz, 0.0314 Hz, and 0.0321 Hz. The distance between the natural frequency is closest to itself: the second order vibration frequency is closest to the natural frequency, the

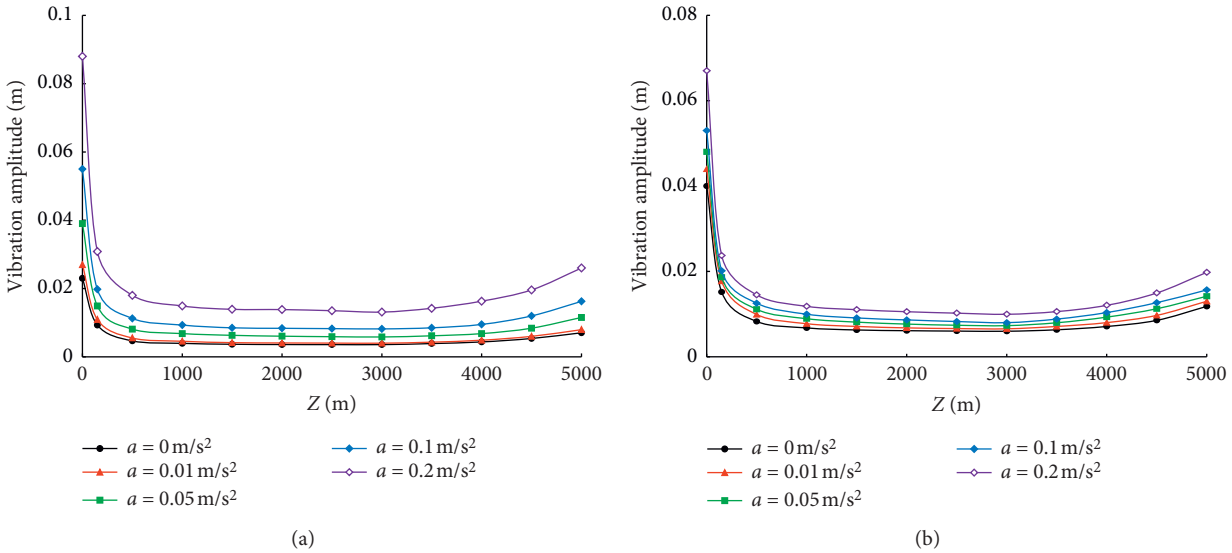

Figure 11: Maximum transverse vibration amplitude connection diagram at different positions of the mining pipe under different towing accelerations. (a) At the constant acceleration stage. (b) At the constant deceleration stage.

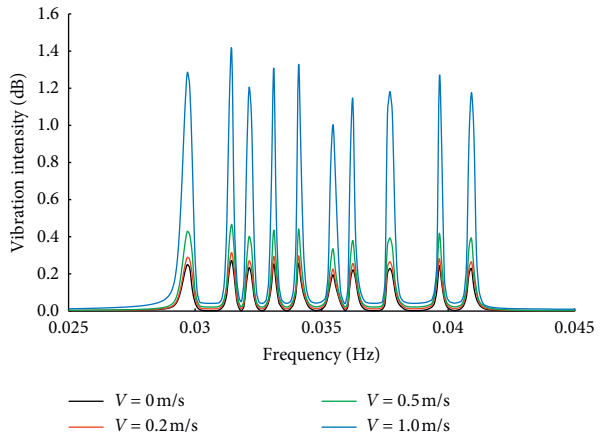

Figure 12: Transverse vibration frequency response under different towing velocities.

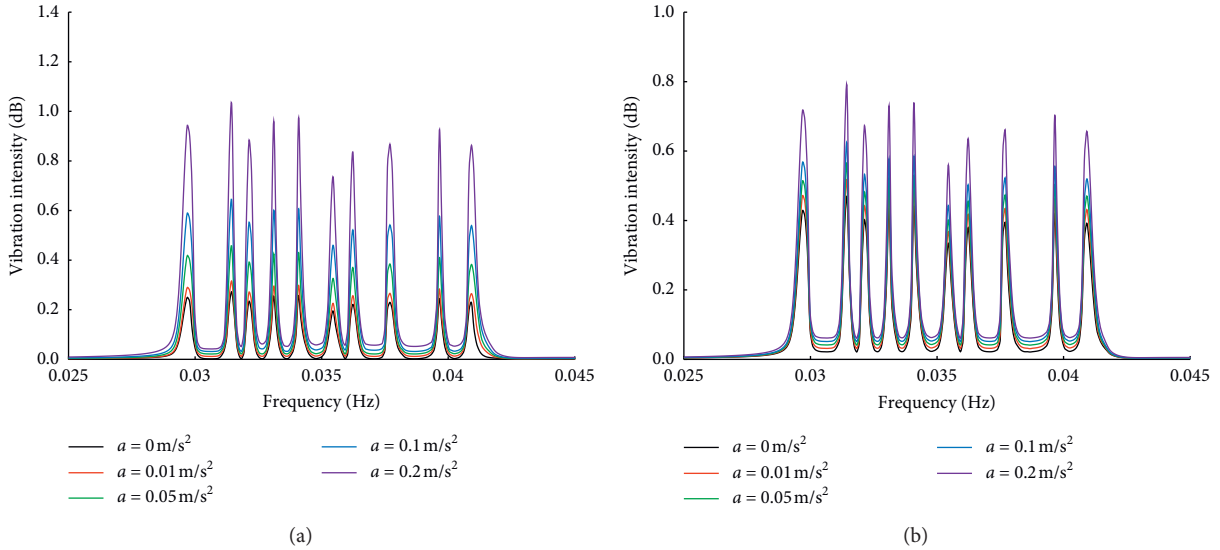

Figure 13: Transverse vibration frequency response under different towing accelerations. (a) At the constant acceleration stage. (b) At the constant deceleration stage.

third order vibration frequency is the farthest from the natural frequency, and the first order vibration frequency is in the middle position.

(1) Under the working wind condition of level 6, when the weight of the ore bin is 30 t, the acceleration is 0.01 m/s^2, and the damping is 0 N · s/mand 200 N · s/m, respectively. The attenuation diagram of the mining pipe vibration intensity during the mining ship constant acceleration and deceleration stages is shown in Figure 14.
Figures 14(a)–14(c) show the vibration intensity attenuation diagram of the mining pipe first three order vibration frequencies in the constant acceleration stage, and Figures 14(d)–14(f) show the vibration intensity attenuation diagram of the mining pipe first three order vibration frequencies in the constant deceleration stage. As shown in Figures 14(a)–14(f), when the acceleration is 0.01 m/s^2 and the damping is 0 N · s/m, the vibration intensity of the first three order vibration frequencies in the constant acceleration stage is 0.3570 dB, 0.3855 dB, and 0.3305 dB, respectively. The vibration intensity of the first three order vibration frequencies in the constant deceleration stage is 0.6519 dB, 0.7082 dB, and 0.5548 dB. After adding 200 N · s/mdamping, the vibration intensity attenuation value of the first three order vibration frequencies in the constant acceleration stage is 0.0679 dB, 0.0709 dB, and 0.0599 dB, respectively, and the attenuation value of the first three order vibration frequencies in the constant deceleration stage is 0.1808 dB, 0.1956 dB, and 0.1139 dB, respectively. It can be seen that in the constant acceleration and deceleration stages, the vibration intensity is the largest at the second order vibration frequency. After adding damping, the amplitude of vibration intensity decreases to the maximum, indicating that the closer the vibration frequency is to the natural frequency, the larger the vibration amplitude is and the more obvious the damping effect is after adding damping.
It can be seen from the comparison between Figures 14(a) and 14(f) that when the acceleration is 0.01 m/s^2, the constant deceleration stage is more sensitive to damping, the vibration intensity attenuation amplitude is greater after adding the same damping, and the vibration reduction effect is more obvious. However, the vibration intensity after vibration reduction in the constant deceleration stage is still greater than that in the constant acceleration stage. Therefore, when the mining ship moves with the acceleration of 0.01 m/s^2, the damping value should be increased in the deceleration stage to reduce the vibration amplitude.

(2) Under the working wind condition of level 6, when the weight of the ore bin is 30 t, the acceleration is 0.1 m/s^2, and the damping is 0 N · s/mand 200 N · s/m, respectively. The attenuation diagram of the mining pipe vibration intensity during the mining ship constant acceleration and deceleration stages is shown in Figure 15.
Figures 15(a)–15(c) show the vibration intensity attenuation diagram of the mining pipe first three order vibration frequencies in the constant acceleration stage, and Figures 15(d)–15(f) show the vibration intensity attenuation diagram of the mining pipe first three order vibration frequencies in the constant deceleration stage. The comparison between Figures 15(a)–15(c) and 10 shows that when the acceleration is 0.1 m/s^2 and the damping is 0 N · s/m, the vibration intensity at the stages of constant acceleration and deceleration is almost the same. After adding 200 N · s/mdamping, the amplitude of vibration intensity reduction at the constant acceleration and deceleration stages differs little, and the decreased amplitude is 0.2260 dB, 0.2645 dB, 0.1424 dB and 0.2177 dB, 0.2603 dB, and 0.1372 dB, respectively. This shows that when the acceleration is 0.1 m/s^2 and the same damping is added in the constant acceleration and deceleration stages, the vibration intensity decreases to the same degree and the vibration reduction effect is the same.

(3) Under the working wind condition of level 6, when the weight of the ore bin is 30 t, the acceleration is 0.2 m/s^2, and the damping is 0 N · s/mand 200 N · s/m, respectively. The attenuation diagram of the mining pipe vibration intensity during the mining ship constant acceleration and deceleration Figures 16(a)–16(c) shows the vibration intensity attenuation diagram of the mining pipe first three order vibration frequencies in the constant acceleration stage, and Figures 16(d)–16(f) show the vibration intensity attenuation diagram of the mining pipe first three order vibration frequencies in the constant deceleration stage. The comparison between Figures 16(a)–16(f) shows that when the acceleration is 0.2 m/s^2 and the damping is 0 N · s/m, the vibration intensity of the first three order frequencies in the constant acceleration stage is 1.3037 dB, 1.4164 dB, and 1.1096 dB, respectively. The vibration intensity of the first three order frequencies in the constant deceleration stage is 0.9926 dB, 1.0950 dB, and 0.8448 dB, respectively. After adding 200 N · s/mdamping, the vibration intensity of the first three order frequencies in the constant acceleration stage is reduced: 0.3616 dB, 0.3912 dB, and 0.2278 dB, respectively, and the vibration intensity of the first three order

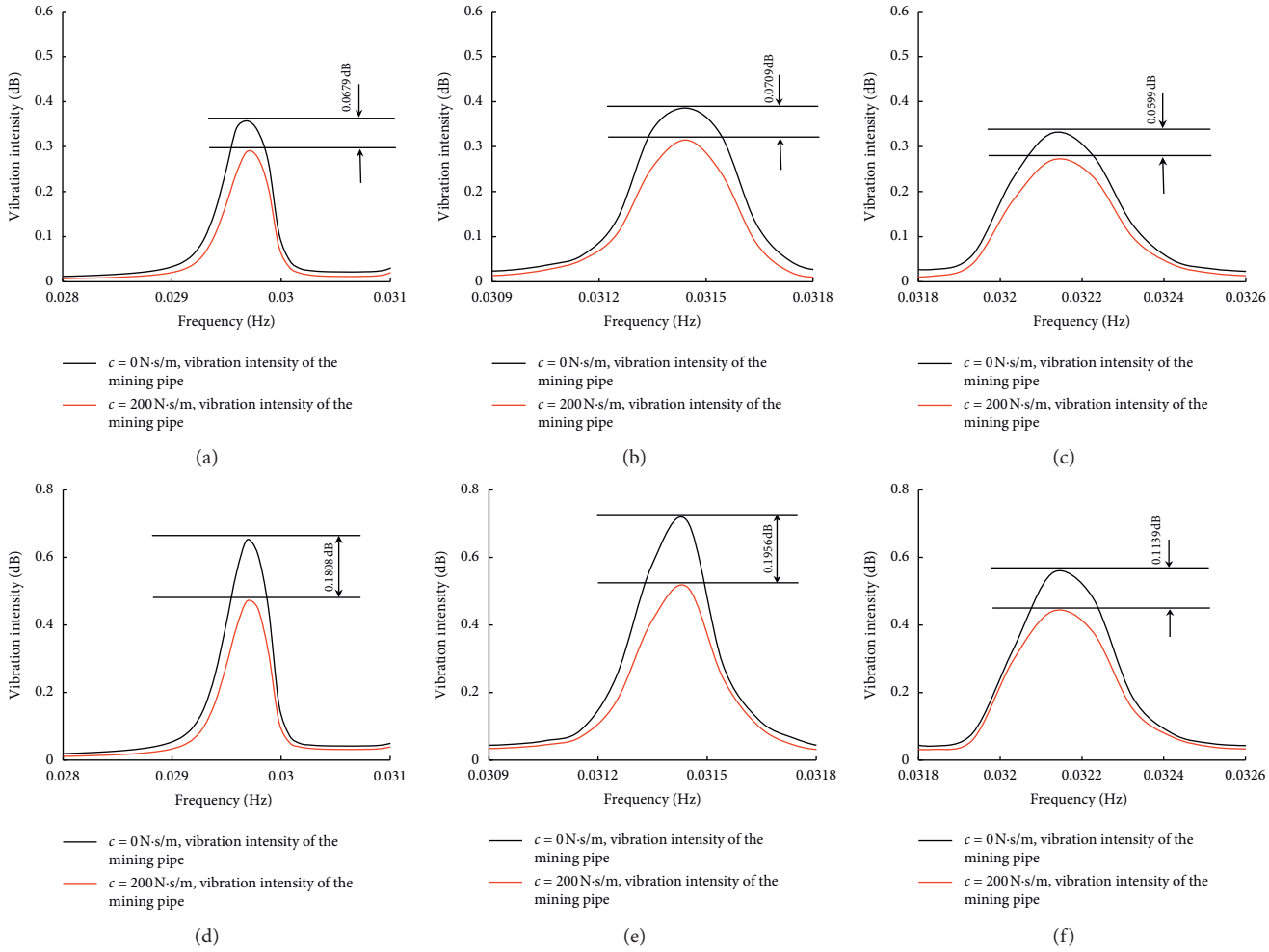

FIGURE 14: $a = 0.01\ \text{m/s}^2$. Transverse vibration intensity attenuation diagram of the mining pipe. (a) The vibration intensity attenuation diagram of the first-order frequency in the constant acceleration stage. (b) The vibration intensity attenuation diagram of the second-order frequency in the constant acceleration stage. (c) The vibration intensity attenuation diagram of the third-order frequency in the constant acceleration stage. (d) The vibration intensity attenuation diagram of the first-order frequency in the constant deceleration stage. (e) The vibration intensity attenuation diagram of the second-order frequency in the constant deceleration stage. (f) The vibration intensity attenuation diagram of the third-order frequency in the constant deceleration stage.

frequencies in the constant deceleration stage is reduced: 0.2753 dB, 0.3145 dB, and 0.1734 dB, respectively. It can be seen from the data analysis that when the acceleration is $0.2\ \text{m/s}^2$, the vibration intensity in the constant acceleration stage is greater than that in the constant deceleration stage. After adding the same damping, the vibration intensity in the constant acceleration stage decreases greatly, indicating that the constant acceleration stage is more sensitive to damping and the vibration reduction effect is more obvious.

(4) Under the working wind condition of level 6, when the weight of the ore bin is 30 t, the acceleration is $0.01\ \text{m/s}^2$ and $0.1\ \text{m/s}^2$, and the damping is $0\ \text{N} \cdot \text{s/m}$ and $200\ \text{N} \cdot \text{s/m}$. The attenuation diagram of the mining pipe vibration intensity during the mining ship constant acceleration and deceleration stages is shown in Figure 17.

(i) Under the working wind condition of level 6, when the weight of the ore bin is 30 t, the towing velocity is 0 m/s, 0.2 m/s, 0.5 m/s, and 1.0 m/s respectively, and the damping is $200\ \text{N} \cdot \text{s/m}$. The transverse vibration frequency of the mining pipe is shown in Figure 12.

As shown in Figure 12, the transverse vibration intensity of the mining pipe increases with the increase of towing velocity, but the change of towing velocity cannot change the transverse vibration frequency of the mining pipe. The vibration intensity corresponding to the first five order vibration frequencies of the mining pipe is relatively large, and the maximum vibration intensity appears at the second order vibration frequency (0.0315 Hz). When the towing velocity is 0 m/s, 0.2 m/s, 0.5 m/s, and 1.0 m/s, the corresponding maximum vibration intensity is 0.2716 dB, 0.3145 dB, 0.4659 dB, and 1.3978 dB, respectively.

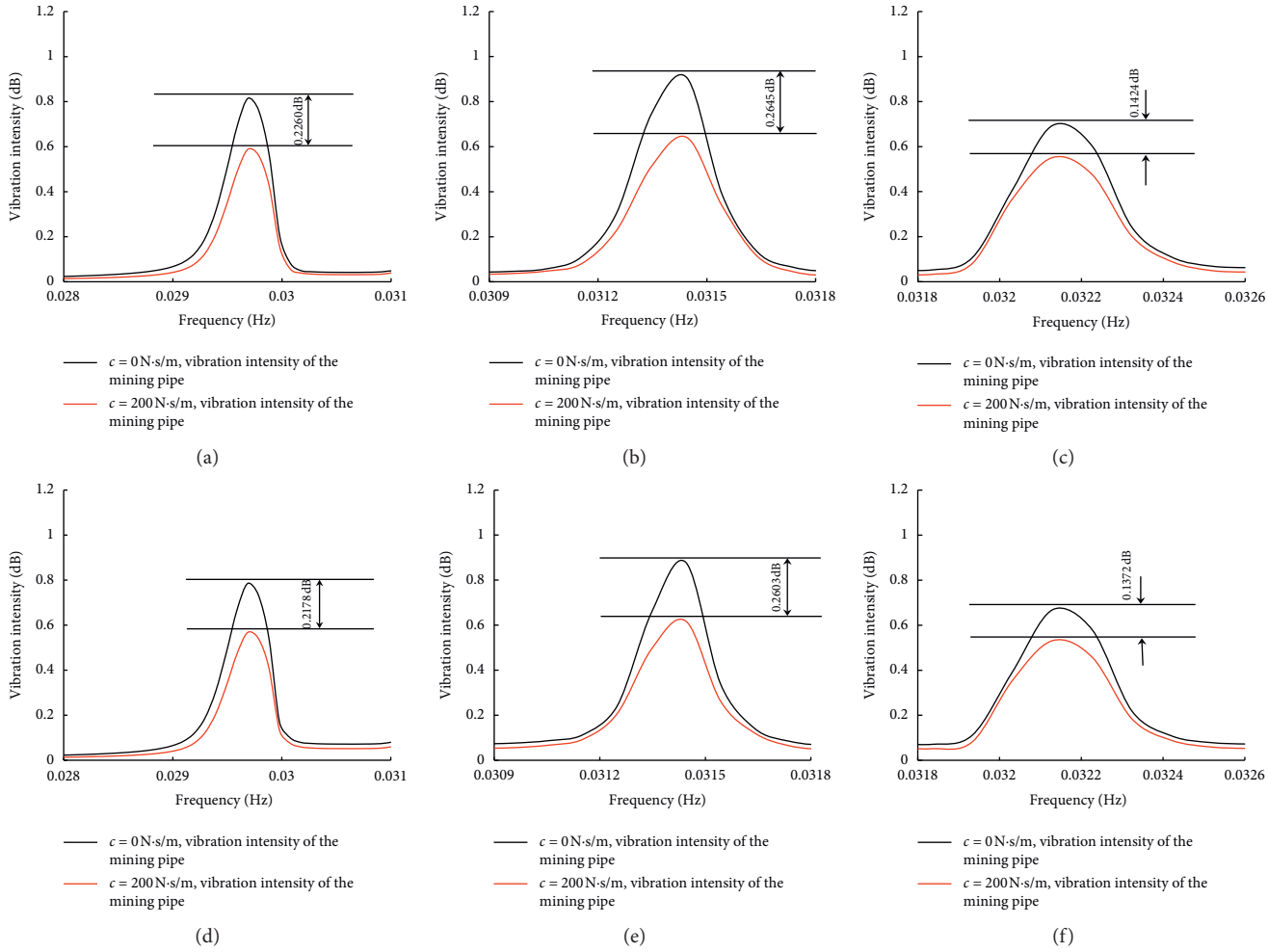

Figure 15: $a = 0.1\ \mathrm{m/s^2}$. Transverse vibration intensity attenuation diagram of the mining pipe. (a) The vibration intensity attenuation diagram of the first-order frequency in the constant acceleration stage. (b) The vibration intensity attenuation diagram of the second-order frequency in the constant acceleration stage. (c) The vibration intensity attenuation diagram of the third-order frequency in the constant acceleration stage. (d) The vibration intensity attenuation diagram of the first-order frequency in the constant deceleration stage. (e) The vibration intensity attenuation diagram of the second-order frequency in the constant deceleration stage. (f) The vibration intensity attenuation diagram of the third-order frequency in the constant deceleration stage.

(ii) Under the working wind condition of level 6, when the weight of the ore bin is 30 t, the towing acceleration is $0\ \mathrm{m/s^2}$, $0.01\ \mathrm{m/s^2}$, $0.05\ \mathrm{m/s^2}$, $0.1\ \mathrm{m/s^2}$, and $0.2\ \mathrm{m/s^2}$, and the damping is $200\ \mathrm{N \cdot s/m}$. The transverse vibration frequency of the mining pipe is shown in Figure 13.

As shown in Figure 13, with the towing acceleration increase, the vibration intensity of the mining pipe is enhanced. Similarly, towing acceleration cannot change the frequency of transverse vibration, and the maximum vibration intensity appears at the second order vibration frequency. When the towing acceleration is $0\ \mathrm{m/s^2}$, $0.01\ \mathrm{m/s^2}$, $0.05\ \mathrm{m/s^2}$, $0.1\ \mathrm{m/s^2}$, and $0.2\ \mathrm{m/s^2}$, the corresponding maximum vibration intensity at the acceleration stage is 0.2715 dB, 0.3145 dB, 0.4543 dB, 0.6406 dB, and 1.0251 dB, respectively. The corresponding maximum vibration intensity at the deceleration stage is 0.4659 dB, 0.5125 dB, 0.5591 dB, 0.6174 dB, and 0.7804 dB, respectively.

(iii) The first three order vibration frequencies are selected as the research object, and the corresponding frequencies are 0.0297 Hz, 0.0314 Hz, and 0.0321 Hz. The distance between the natural frequency is closest to itself: the second order vibration frequency is closest to the natural frequency, the third order vibration frequency is the farthest from the natural frequency, and the first order vibration frequency is in the middle position.

(1) Under the working wind condition of level 6, when the weight of the ore bin is 30 t, the acceleration is $0.01\ \mathrm{m/s^2}$, and the damping is $0\ \mathrm{N \cdot s/m}$ and $200\ \mathrm{N \cdot s/m}$, respectively. The attenuation diagram of the mining pipe vibration intensity during the mining ship constant

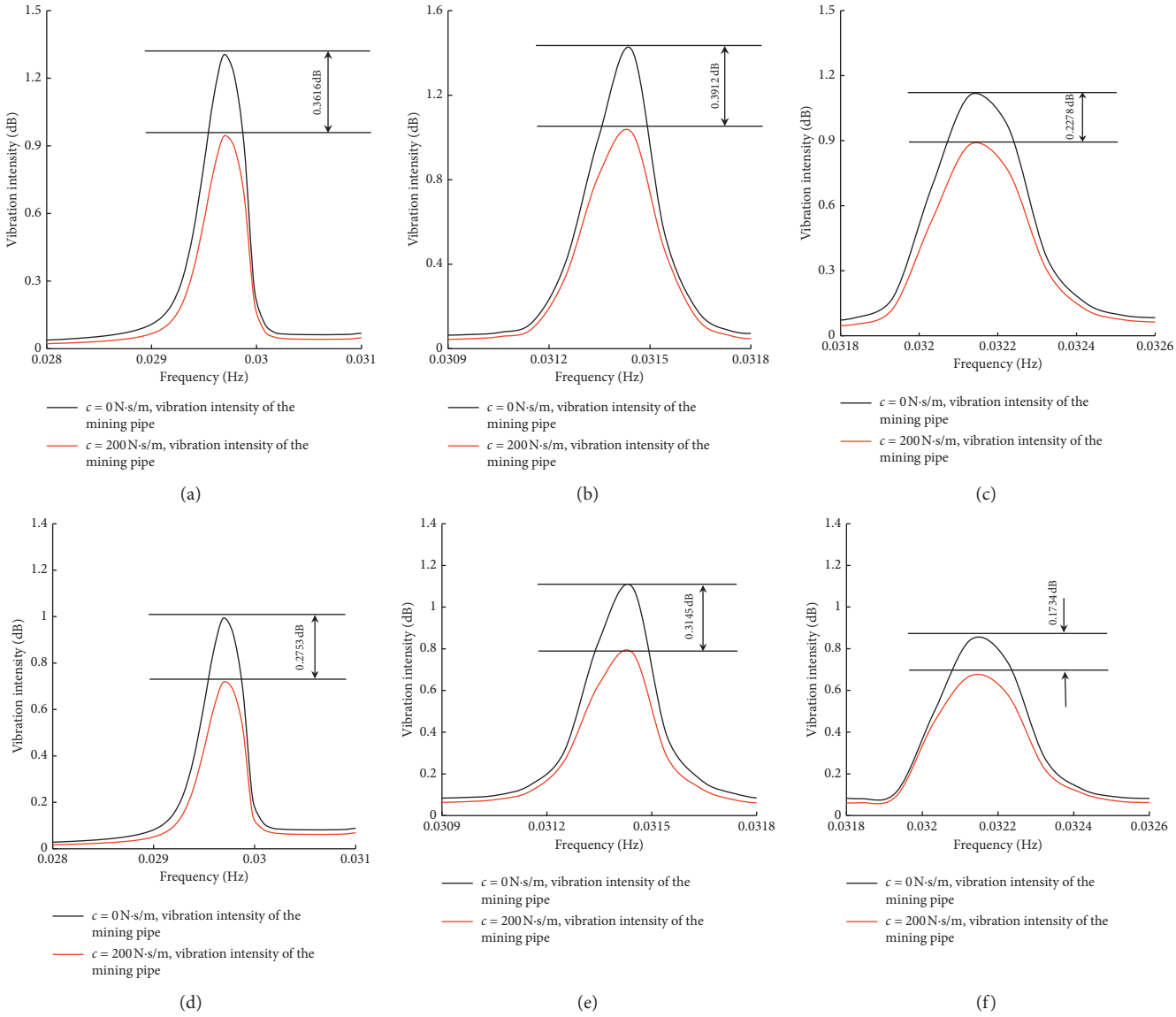

Figure 16: $a = 0.2\ \mathrm{m/s^2}$. Transverse vibration intensity attenuation diagram of the mining pipe. (a) The vibration intensity attenuation diagram of the first-order frequency in the constant acceleration stage. (b) The vibration intensity attenuation diagram of the second-order frequency in the constant acceleration stage. (c) The vibration intensity attenuation diagram of the third-order frequency in the constant acceleration stage. (d) The vibration intensity attenuation diagram of the first-order frequency in the constant deceleration stage. (e) The vibration intensity attenuation diagram of the second-order frequency in the constant deceleration stage. (f) The vibration intensity attenuation diagram of the third-order frequency in the constant deceleration stage.

acceleration and deceleration stages is shown in Figure 14.

Figures 14(a)–14(c) show the vibration intensity attenuation diagram of the mining pipe first three order vibration frequencies in the constant acceleration stage, and Figures 14(d)–14(f) show the vibration intensity attenuation diagram of the mining pipe first three order vibration frequencies in the constant deceleration stage. As shown in Figures 14(a)–14(f), when the acceleration is $0.01\ \mathrm{m/s^2}$ and the damping is $0\ \mathrm{N \cdot s/m}$, the vibration intensity of the first three order vibration frequencies in the constant acceleration stage is 0.3570 dB, 0.3855 dB, and 0.3305 dB, respectively. The vibration intensity of the first three order vibration frequencies in the constant deceleration stage is 0.6519 dB, 0.7082 dB, and 0.5548 dB. After adding $200\ \mathrm{N \cdot s/m}$damping, the vibration intensity attenuation value of the first three order vibration frequencies in the constant acceleration stage is 0.0679 dB, 0.0709 dB, and 0.0599 dB, respectively, and the attenuation value of the first three order vibration frequencies in the constant deceleration stage is 0.1808 dB, 0.1956 dB, and 0.1139 dB, respectively. It can be

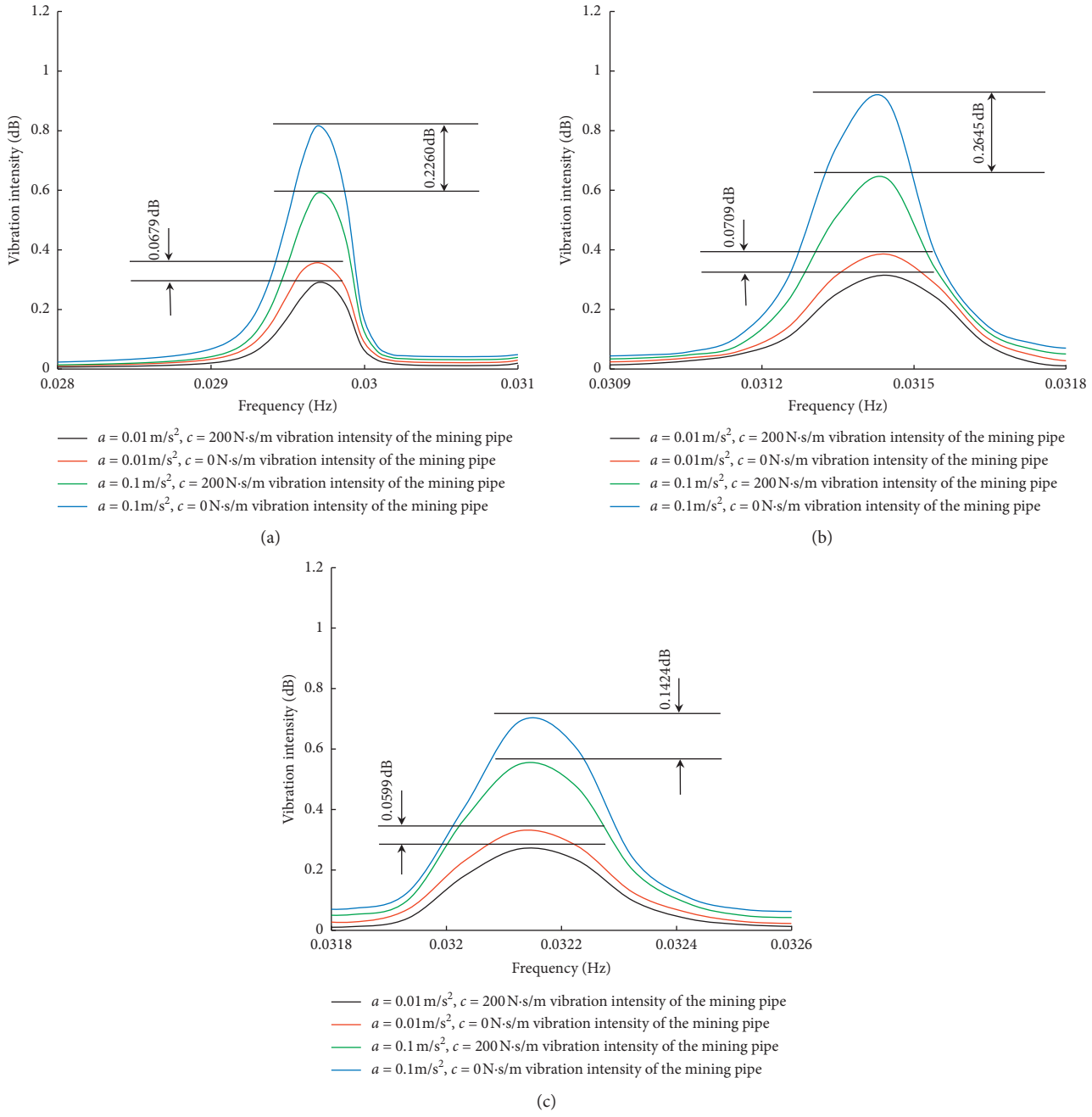

FIGURE 17: $a = 0.2\ \text{m/s}^2$. Transverse vibration intensity attenuation diagram of the mining pipe in the constant acceleration stage. (a) The vibration intensity attenuation diagram of the first-order frequency. (b) The vibration intensity attenuation diagram of the second-order frequency. (c) The vibration intensity attenuation diagram of the third-order frequency.

seen that in the constant acceleration and deceleration stages, the vibration intensity is the largest at the second order vibration frequency. After adding damping, the amplitude of vibration intensity decreases to the maximum, indicating that the closer the vibration frequency is to the natural frequency, the larger the vibration amplitude is and the more obvious the damping effect is after adding damping.

It can be seen from the comparison between Figures 14(a) and 14(f) that when the acceleration is $0.01\ \text{m/s}^2$, the constant deceleration stage is more sensitive to damping, the vibration intensity attenuation amplitude is greater after adding the same damping, and the vibration reduction effect is more obvious. However, the vibration intensity after vibration reduction in the constant deceleration stage is still greater than that in the constant acceleration stage. Therefore, when the mining ship moves with the acceleration of $0.01\ \text{m/s}^2$, the damping value should be increased in the

deceleration stage to reduce the vibration amplitude.

(2) Under the working wind condition of level 6, when the weight of the ore bin is 30 t, the acceleration is 0.1 m/s^2, and the damping is 0 N · s/mand 200 N · s/m, respectively. The attenuation diagram of the mining pipe vibration intensity during the mining ship constant acceleration and deceleration stages is shown in Figure 15.

Figures 15(a)–15(c) show the vibration intensity attenuation diagram of the mining pipe first three order vibration frequencies in the constant acceleration stage, and Figures 15(d)–15(f) show the vibration intensity attenuation diagram of the mining pipe first three order vibration frequencies in the constant deceleration stage. The comparison between Figures 15(a)–15(c) and 10 shows that when the acceleration is 0.1 m/s^2 and the damping is 0 N · s/m, the vibration intensity at the stages of constant acceleration and deceleration is almost the same. After adding 200 N · s/mdamping, the amplitude of vibration intensity reduction at the constant acceleration and deceleration stages differs little, and the decreased amplitude is 0.2260 dB, 0.2645 dB, 0.1424 dB and 0.2177 dB, 0.2603 dB, and 0.1372 dB, respectively. This shows that when the acceleration is 0.1 m/s^2 and the same damping is added in the constant acceleration and deceleration stages, the vibration intensity decreases to the same degree and the vibration reduction effect is the same.

(3) Under the working wind condition of level 6, when the weight of the ore bin is 30 t, the acceleration is 0.2 m/s^2, and the damping is 0 N · s/mand 200 N · s/m, respectively. The attenuation diagram of the mining pipe vibration intensity during the mining ship constant acceleration and deceleration Figures 16(a)–16(c) shows the vibration intensity attenuation diagram of the mining pipe first three order vibration frequencies in the constant acceleration stage, and Figures 16(d)–16(f) show the vibration intensity attenuation diagram of the mining pipe first three order vibration frequencies in the constant deceleration stage. The comparison between Figures 16(a)–16(f) shows that when the acceleration is 0.2 m/s^2 and the damping is 0 N · s/m, the vibration intensity of the first three order frequencies in the constant acceleration stage is 1.3037 dB, 1.4164 dB, and 1.1096 dB, respectively. The vibration intensity of the first three order frequencies in the constant deceleration stage is 0.9926 dB, 1.0950 dB, and 0.8448 dB, respectively. After adding 200 N · s/mdamping, the vibration intensity of the first three order frequencies in the constant acceleration stage is reduced: 0.3616 dB, 0.3912 dB, and 0.2278 dB, respectively, and the vibration intensity of the first three order frequencies in the constant deceleration stage is reduced: 0.2753 dB, 0.3145 dB, and 0.1734 dB, respectively. It can be seen from the data analysis that when the acceleration is 0.2 m/s^2, the vibration intensity in the constant acceleration stage is greater than that in the constant deceleration stage. After adding the same damping, the vibration intensity in the constant acceleration stage decreases greatly, indicating that the constant acceleration stage is more sensitive to damping and the vibration reduction effect is more obvious.

(4) Under the working wind condition of level 6, when the weight of the ore bin is 30 t, the acceleration is 0.01 m/s^2 and 0.1 m/s^2, and the damping is 0 N · s/mand 200 N · s/m. The attenuation diagram of the mining pipe vibration intensity during the mining ship constant acceleration and deceleration stages is shown in Figure 17.

As shown in Figure 17, the larger the acceleration is, the stronger the vibration intensity will be; when the same damping is added, the vibration intensity decreases more. However, after adding damping, the vibration intensity with large acceleration is still greater than that with small acceleration, so the mining ship should try to keep the acceleration as small as possible during the constant acceleration or deceleration motion.

5. Conclusions

In this paper, the transverse vibration characteristics of the 5000 m ladder-shaped mining pipe is analyzed. The mining pipe is simplified into the beam element, which is discretized based on the finite element method and calculated by the Wilson-θ direct integral method. The main conclusions are as follows.

(1) The transverse vibration of the mining pipe is irregular movement and causes the oscillation phenomenon. The overall vibration trend decreases first and then increases. The maximum vibration amplitude appears at the top of the mining pipe and the minimum vibration amplitude appears at 3000 m of the mining pipe. The vibration velocity and acceleration also have the same motion law.

(2) Under the same working wind conditions, increasing the towing velocity will increase the mining pipe overall transverse vibration amplitude. Whether in the stage of constant acceleration and deceleration, increasing the towing acceleration will also increase the overall vibration amplitude of the mining pipe.

(3) Under the working wind condition of level 6, when the ore bin weight, towing velocity, and additional damping are unchanged and the acceleration is 0.01 m/s^2, the constant deceleration stage is more

sensitive to damping. After damping is added, the vibration intensity attenuation amplitude is large and the damping effect is more obvious. However, the vibration intensity after damping is still greater than that without damping in the constant acceleration stage, so the damping value should be increased during the constant deceleration stage. When the acceleration reaches $0.1\,m/s^2$, after damping is added, the vibration intensity drops to the same degree at the stage of constant acceleration and deceleration, and the vibration reduction effect is basically the same. When the acceleration reaches $0.2\,m/s^2$, the vibration intensity attenuates greatly in the constant acceleration stage after damping is added, and in the constant acceleration stage the vibration reduction effect is more obvious.

(4) The vibration intensity produced by the large acceleration with damping added is still greater than vibration intensity produced by the small acceleration without damping added. Therefore, the mining ship should keep the small acceleration for towing motion.

Data Availability

The data used to support the findings of this study are available from the corresponding author upon request.

Conflicts of Interest

The authors declare that there are no conflicts of interest.

Acknowledgments

This work was supported by the National Natural Science Foundation of China (allotment grant number 51774193) and the Shandong Provincial Natural Science Foundation, China (allotment grant number ZR2017MEE025)

References

[1] L. Liu, *Research on Dynamic Performance of Solid-Liquid Two-phase Flow in Hydraulic Transport in Deep Sea Mining*, Shanghai Jiao Tong University, Shanghai, China, 2019.

[2] W. Song, *Mechanical Analysis of Lifting Hard Pipe in Deep Sea Mining and Design of Collector*, Southwest Petroleum University, Chengdu, China, 2018.

[3] Y. Fu, *Study on Hose Conveying Characteristics in Deep Sea Mining*, Minzu University of China, Beijing, China, 2019.

[4] R. C. Xin, H. Liu, and X. Guan, *Marine Resources*, Chemical Industry Press, Beijing, China, 2013.

[5] Y. Deng. Software, *Design for Spatial Configuration and Dynamic Analysis of Flexible Pipeline in Deep Sea Mining System*, Xiangtan University, Xiangtan, China, 2017.

[6] Y. L. Feng, Y. Xu, and F. Z. Feng, "Experimental study for lateral motion of 1 km articulated lifting subsystem," *Journal of China University of Mining Technology*, no. 02, pp. 246–250, 2007.

[7] J. S. Chung, "Deep-ocean mining technology: learning curve I," in *Proceedings of the Fifth ISOPE Ocean Mining Symposium*, Tsukuba, Japan, September 2003.

[8] B. R. Cheng, J. S. Chung, and Z. C. Zheng, "Effects of flexible joints on the 3-D nonlinear coupled responses of a long vertical pipe," in *Proceedings of the Fifth International Offshore and Polar Engineering Conference*, The Hague, The Netherlands, June 1995.

[9] E. Haluk, "Vibration analysis of stepped-pipe strings for mining from deep-sea floors," *Ocean Engineering*, vol. 32, no. 1, pp. 37–55, 2005.

[10] S. Hong and H. W. Kim, "Coupled dynamic analysis of underwater tracked vehicle and long flexible pipe," in *Proceedings of the 6th Ocean Mining Symposium*, pp. 132–140, ISOPE, Changsha, China, October 2005.

[11] C. Yoo, Y. Chan, D. K. Lee et al., "Behavior of deep sea mining pipe and its effect on internal flow," in *Proceedings of the Fifth ISOPE Ocean Mining Symposium*, Tsukuba, Japan, September 2003.

[12] H. L. Xu, X. Rao, and F. Q. Yang, "Influence of lateral swing on transportation characteristics of deep sea mining pipeline," *Journal of Central South University (Science and Technology)*, vol. 50, no. 10, pp. 2395–2402, 2019.

[13] Y. Li, *Dynamic Analysis of 1000 m Ocean Pilot Mining System Based on Three-Dimensional Discrete Element Method Pipe Model*, Central South University, Changsha, China, 2009.

[14] J. Liu, J. L. Mao, and B. Y. Liu, "Dynamic analysis for the lateral movement of a lifting pipe in deep sea mining," *Engineering Sciences*, no. 11, pp. 74–79, 2001.

[15] X. Y. Qiu, *Research for Passive Control for Longitudinal Vibration of Lifting Pipe in Deep Sea Mining System*, Central South University, Changsha, China, 2014.

[16] L. J. Xiao, Q. Liu, and B. Liang, "Longitudinal vibration analysis of mining pipe in deep sea mining based on wave current combined action," *Mining Research and Development*, vol. 39, no. 11, pp. 147–150, 2019.

[17] L. J. Li, *Design and Control of Active Heave Compensation System for Dynamic Vibration Absorbing Deep-Sea Mining*, Central South University, Changsha, China, 2012.

[18] Z. Wang, *Fluid-solid Coupling Analysis and Comprehensive Evaluation of the Working Characteristics of the Uplift Pipeline in Deep Sea Mining*, Central South University, Changsha, China, 2010.

[19] Y. Li, G. C. Jia, and S. J. Liu, "Mechanical characteristics on long lifting pipeline in deep-ocean mining considering fluid-structure interaction," *Journal of Central South University (Science and Technology)*, vol. 47, no. 11, pp. 3670–3676, 2016.

[20] B. Liang, J. L. Xu, and T. W. Zhai, "Finite element analysis of longitudinal vibration of hoisting pipe in deep sea mining," *Mining Research and Development*, vol. 39, no. 01, pp. 106–109, 2019.

[21] Q. Liu and L. J. Xiao, "Analysis and research on longitudinal vibration characteristics of deep sea mining pipe based on finite element method," *Mathematical Problems in Engineering*, vol. 2020, Article ID 8219794, 18 pages, 2020.

[22] X. C. Wang, *Finite Element Method*, Tsinghua University Press, Beijing, China, 2015.

[23] Q. K. Du and J. R. Chen, *The Mathematical Theory of Finite Element Methods*, Science Press, Beijing, China, 2012.

[24] P. Zeng, *Finite Element Basic Course*, Higher Education Press, Beijing, China, 2017.

[25] R. Q. Xu, *Finite Element Method of Structural Analysis and MATLAB Program Design*, China Communications Press, Beijing, China, 2005.

[26] C. H. Wang, Y. Y. Feng, K. Yue, and X. X. Zhang, "Discontinuous finite element method for combined radiation-conduction heat transfer in participating media,"

International Communications in Heat and Mass Transfer, vol. 108, Article ID 104287, 2019.

[27] Y. Y. Feng and C. H. Wang, "Discontinuous finite element method applied to transient pure and coupled radiative heat transfer," *International Communications in Heat and Mass Transfer*, vol. 122, Article ID 105156, 2021.

[28] Q. Hu, *The Simulation Test Research on Mechanical Behavior of the Lifting Pipe System of Deep-Ocean Mining*, Central South University, Changsha, China, 2010.

[29] T. C. Feng, *Ship Swaying & Manipulating*, National Defense Industry Press, Beijing, China, 1989.

[30] L. J. Xiao, W. M. Zhang, and M. Fang, "Study on nonlinear dynamic characteristics of hoisting pipe in deep sea mining," *Journal of Coal*, no. 04, pp. 417–421, 2002.

[31] L. J. Xiao, *Study on Kinematics and Dynamics Characteristics of Deep Ocean Mining Pipe*, University of Science and Technology Beijing, Beijing, China, 2000.

[32] G. Wang, *Research on Spatial Configuration and Dynamic Characteristics of Hoisting Pipeline System in Deep-Sea Mining Operations*, Central South University, Changsha, China, 2009.

[33] S. Q. Wang and B. C. Ling, *Ocean Engineering Wave Mechanics*, Ocean university of China press, Qingdao, China, 2013.

[34] S. T. Santillan and L. N. Virgin, "Numerical and experimental analysis of the static behavior of highly deformed risers," *Ocean Engineering*, vol. 38, no. 3, pp. 1397–1402, 2011.

[35] X. S. Lu, *Advancd Dynamics of Structures*, Shanghai Jiao Tong University Press, Shanghai, China, 1992.

[36] Z. W. Cai, *Wave Theory and its Engineering Application*, National University of Defense Technology Press, Changsha, China, 2000.

[37] H. W. Liu, *Mechanics of Materials*, Higher Education Press, Beijing, China, 2011.

[38] Q. Wu, J. M. Yang, H. N. Lu et al., "Effects of heave motion on the dynamic performance of vertical transport system for deep sea mining," *Applied Ocean Research*, no. 101, pp. 1–11, 2020.

[39] B. Xu, Y. F. Gao, and L. Yu, *MATLAB Finite Element Structural Dynamics Analysis and Engineering Application*, Tsinghua University Press, Beijing, China, 2009.

[40] M. A. Li and L. Qian, *MATLAB/SIMULINK Dynamics System Modeling and Simulation*, National Defense Industry Press, Beijing, China, 2015.

[41] Z. J. Zhou, N. Yang, and A. J. Liu, "Study on the application of axial displacement of hard pipe in step uplift," in *Proceedings of the 17th China Ocean Engineering Symposium*, pp. 536–539, China Ocean Engineering Society, Nanning, China, 2015.

[42] Y. Li, K. F. Liao, and F. Lu, "Dynamic analysis of 1000 m deep-sea uplift hard tube considering fluid-solid coupling," *Journal of Water Resources and Water Engineering*, vol. 28, no. 01, pp. 163–168, 2017.

[43] N. Q. Hu, *Mechanical Vibration*, National University of Defense Technology Press, Changsha, China, 2017.